Title

Cometabolism of 17α-ethynylestradiol by nitrifying bacteria depends on reducing power availability and leads to elevated nitric oxide formation

Authors

Sheng, Qi
Yi, Ming
Men, Yujie
et al.

Publication Date

2021-08-01

DOI

10.1016/j.envint.2021.106528

Environment International 153 (2021) 106528

Contents lists available at ScienceDirect

Environment International

journal homepage: www.elsevier.com/locate/envint

Cometabolism of 17α-ethynylestradiol by nitrifying bacteria depends on reducing power availability and leads to elevated nitric oxide formation

Qi Sheng [a], Ming Yi [a], Yujie Men [b], Huijie Lu [a,*]

[a] Key Laboratory of Environment Remediation and Ecological Health, Ministry of Education, College of Environmental and Resource Sciences, Zhejiang University, Hangzhou 310058, China
[b] Department of Chemical and Environmental Engineering, University of California, Riverside, CA 92521, United States

ARTICLE INFO

Handling Editor: Dr. Guo-Ping Sheng

Keywords:
Cometabolism
17α-ethynylestradiol
Reductant model
Nitric oxide
nirK
Nitrosomonas europaea

ABSTRACT

17α-ethynylestradiol (EE2) is a priority emerging contaminant (EC) in diverse environments that can be cometabolized by ammonia oxidizing bacteria (AOB). However, its transformation kinetics and the underlying molecular mechanism are unclear. In this study, kinetic parameters, including maximum specific EE2 transformation rate, EE2 half-saturation coefficient, and EE2 transformation capacity of AOB were obtained by using the model AOB strain, *Nitrosomonas europaea* 19718. The relationship between EE2 cometabolism and ammonia oxidation was divided into three phases according to reducing power availability, namely "activation", "coupling", and "saturation". Specifically, there was a universal lag of EE2 transformation after ammonia oxidation was initiated, suggesting that sufficient reducing power (approximately 0.95 ± 0.06 mol NADH/L) was required to activate EE2 cometabolism. Interestingly, nitric oxide emission increased by 12 ± 2% during EE2 cometabolism, along with significantly upregulated *nirK* cluster genes. The findings are of importance to understanding the cometabolic behavior and mechanism of EE2 in natural and engineered environments. Maintaining relatively high and stable reducing power supply from ammonia oxidation can potentially improve the cometabolic removal of EE2 and other ECs during wastewater nitrification processes.

1. Introduction

The growing concerns on steroid hormones as a kind of emerging contaminants (ECs) in aquatic environment are attributed to their potential risks to ecosystems and human health (Gavrilescu et al., 2015; Hamid and Eskicioglu, 2012; Luo et al., 2014; Petrie et al., 2015). 17α-ethynylestradiol (EE2) is a synthetic estrogen commonly used in oral contraceptive pills (700 kg/year), and is the main contributor to estrogenic activity in the environment causing alterations in reproductive behaviors of diverse aquatic organisms (Adeel et al., 2017; Caldwell et al., 2012; Laurenson et al., 2014; Tetreault et al., 2011), making it one of the priority ECs on the EU Watch list in Decision 2015/495/EU (Nguyen et al., 2020). EE2 enters into the environment mainly via domestic wastewater discharge, leading to its ubiquitous distribution in different water environments at concentrations up to 230 ng/L (Adeel et al., 2017; Luo et al., 2014; Pauwels et al., 2008).

Cometabolic biodegradation by ammonia oxidizing bacteria (AOB) represents a major pathway of EE2 removal in natural and engineered systems, e.g., wastewater treatment plants (WWTPs) (Forrez et al., 2009; Khunjar et al., 2011; Shi et al., 2004; Skotnicka-Pitak et al., 2009). Although positive correlations between EE2 biotransformation rates and nitrification activity have been repeatedly found by using nitrifying activated sludge and AOB (Jantanaprasartporn et al., 2018; Yi and Harper, 2007), the molecular mechanism of EE2 cometabolism remains elusive. Ammonia monooxygenase (AMO) has been suggested as the key enzyme participating in EE2 cometabolism, due to two possible reasons: 1) inhibiting AMO by allylthiourea (ATU) significantly reduced EE2 cometabolic activity (Gusseme et al., 2009; Laurenson et al., 2014; Yi and Harper, 2007); 2) one of the EE2 transformation products (TPs), OH-EE2 with a hydroxyl group on the aromatic ring A or polycyclic B of EE2 is formed during AMO-catalyzed ammonia hydroxylation to hydroxylamine (Khunjar et al., 2011; Yi and Harper, 2007). However, the involvement of other enzymes in regulating cometabolic removal of EE2 cannot be excluded. A recent study has underlined the non-specific inhibition of ATU on copper-containing enzymes other than AMO (Men et al., 2017), indicating that the contributions of other enzymes to EE2 biotransformation might be underestimated. At the transcriptional level, both up- and down-regulations of *amoA* have been reported during the

* Corresponding author at: College of Environmental and Resource Sciences, Zhejiang University, 866 Yu Hang Tang Rd, Hangzhou, China.
E-mail address: luhuijie@zju.edu.cn (H. Lu).

https://doi.org/10.1016/j.envint.2021.106528
Received 14 December 2020; Received in revised form 8 March 2021; Accepted 13 March 2021
Available online 25 March 2021

cometabolism of organic ECs by the traditional reverse transcription-quantitative PCR (RT-qPCR) assays (Wang et al., 2019a; b). A better understanding of the molecular mechanism of EE2 cometabolism could be facilitated by high-throughput gene expression analysis, e.g., RNA-seq. Lastly, the existence of diverse biotic TPs of EE2 (Barr et al., 2012; Skotnicka-Pitak et al., 2009), e.g., sulfo-EE2, also suggests the potential involvement of enzymes other than AMO.

Reductants generated from primary substrate utilization, e.g., nicotinamide-adenine dinucleotide (NADH), could represent a limiting factor for EC cometabolism. During EE2 cometabolism by nitrifying activated sludge, supplying more reductants by increasing initial ammonia concentrations promoted EE2 removal (Jantanaprasartporn et al., 2018). The addition of alternative energy sources, e.g., hydrazine, can also enhance EE2 transformation by alleviating reducing power deficiency (Vader et al., 2000). Nonetheless, there is a lack of quantitative information on the required reducing power of EE2 cometabolism by AOB. The detailed correlation between ammonia oxidation and EE2 cometabolism under limited reducing power supply also desires further investigation. Traditional first-order or pseudo-first-order kinetics have been applied to describe EE2 cometabolism (Hamid and Eskicioglu, 2012; Shi et al., 2004), which did not link cometabolic substrate removal with primary substrate consumption. Alternatively, the reductant model takes into account primary substrate as a co-limiting factor, which supplies reducing power to the cometabolic process (Delgadillo-Mirquez et al., 2011; Fernandez-Fontaina et al., 2014). The model outperforms other methods in modeling cometabolic processes in later studies (Liu et al., 2015), especially for chlorinated and brominated aliphatic hydrocarbons (Jesus et al., 2016).

Critical knowledge gaps remain in EE2 cometabolism by AOB: 1) how the cometabolic process correlates with the oxidation of ammonia based on reducing power availability; 2) what are the kinetics of EE2 cometabolism based on the reductant model; 3) what genes are involved in regulating the cometabolic transformation of EE2. This study aims to fill the above gaps by evaluating EE2 cometabolic behaviors, obtaining cometabolic kinetics, identifying EE2 TPs and the differentially expressed genes during EE2 cometabolism by the model AOB, *Nitrosomonas europaea*. Outcomes from this study are expected to provide new insights into understanding the cometabolism of broader ECs and enhancing their removals by nitrifying bacteria at WWTPs and in the natural environment.

2. Materials and methods

2.1. Cultivation of Nitrosomonas europaea

Nitrosomonas europaea ATCC 19718 was cultivated as previously described (Yu and Chandran, 2010). Briefly, the culture was grown at 30℃ and shaken in dark at 150 rpm in a growth medium containing 280 mg N/L and trace elements (per liter): 0.2 g of $MgSO_4{\cdot}7H_2O$, 0.02 g of $CaCl_2{\cdot}2H_2O$, 0.087 g of K_2HPO_4, 2.52 g HEPPS (3-[4-(2-Hydroxyethyl)-1-piperazine] propanesulfonic acid), 0.85 g $KHCO_3$, 1 mL of 13% EDTA-Fe (III), 1 mL of trace elements solution (10 mg of $Na_2MoO_4{\cdot}2H_2O$, 17.2 mg of $MnSO_4{\cdot}H_2O$, 10 mg of $ZnSO_4{\cdot}7H_2O$, 0.4 mg of $CoCl_2{\cdot}6H_2O$, and 100 mL of distilled water), and 0.5 mL of 1 mM $CuSO_4{\cdot}5H_2O$. Reactor pH was controlled in the range of 6.8–7.8 by manual addition of filter-sterilized 2 M $KHCO_3$ solution. Dissolved oxygen (DO) was maintained at 2–3 mg/L.

2.2. EE2 biotransformation in batch and chemostat experiments

EE2 was purchased from Dr. Ehrenstorfer GmbH (Augsburg, Germany). Pre-grown *N. europaea* culture at late exponential phase was harvested and washed with fresh medium without ammonia to remove residual nitrite and concentrate the biomass. Concentrated culture was thoroughly mixed and resuspended in 500 mL medium containing 200 μg/L EE2 and 280 mg/L NH_4^+-N. Ammonia, nitrite, and EE2 concentrations were monitored every 12 h for 3 days, and 15 mL biomass was sampled for RNA-seq at t = 24 h when the transformation rate of EE2 was the highest. Control groups without biomass and with heat-inactivated biomass (121℃ and 103 kPa for 30 min) were set up to characterize self-degradation and adsorption of EE2, respectively. Four hundred mL batch cultures were sampled at t = 24 h in all groups for TP identification. All batch experiments were conducted in triplicate. In order to further understand the correlation between primary metabolism and cometabolism under varied reducing power availability, a series of copper inhibition tests were conducted, where 20, 50, and 100 μg/L Cu^{2+} were added to *N. europaea* cells so that different levels of reducing power supply were created (detailed experimental procedure can be found in Supplementary Material).

The chemostat was started with a batch period (2 L, 30℃, 3 days in dark), and then switched to chemostat operation with a hydraulic retention time (HRT) of 2 d and constant aeration at 1 L/min. The pH was controlled at 7.50 ± 0.20 by automatic addition of sterile $KHCO_3$ solution (2 M). Chemostat medium was the same as that in the batch experiments above, except no EE2 was added. Ammonia and nitrite concentrations were monitored every 12 h until the reactor reached a steady state on day 5 and lasted 2 days. Subsequently, 400 μg/L EE2 was added into the medium, and the chemostat was operated for another 9 days. Effluent was sampled before and 2, 5, 7 days after EE2 addition (labelled as “no EE2”, and “2d”, “5d”, “7d” with EE2, respectively) for TP identification and RT-qPCR analysis.

2.3. Measurement of nitrogenous species and EE2

NH_4^+-N and NO_2^--N concentrations were measured according to standard methods (China, 2002). Biomass concentration was determined by cell count (6.3×10^{12} cells/g dry mass for *Nitrosomonas*) which can be calculated from optical density (OD600 1.00 converts to 1.01×10^9 cells/mL) (Farges et al., 2012). Gaseous NO (nCLD AL, Ecophysics, USA) and nitrous oxide (N_2O) (Agilent 7890A-5977B, USA) in the headspace of the chemostat reactor were measured once per 12 h (details in Supplementary Material).

EE2 was quantified using Prominence high-performance liquid chromatograph system equipped with a fluorescence detector (HPLC-FLD) (Shimadzu LC-20AD, Japan). A ZORBAX Eclipse XDB-C18 column (150 mm × 4.6 mm, 5 μm, Agilent) was used for separation at 40℃. The mobile phase consisted of water/acetonitrile (50:50, v/v) at a flow rate of 1.0 mL/min. The injection volume was 10 μL. Fluorescence detection of EE2 was at an excitation wavelength of 280 nm and an emission wavelength of 310 nm (Lima et al., 2013).

2.4. Identification of EE2 transformation products

Samples from batch (t = 24 h) as well as chemostat (before and day 2, 5, 7 after EE2 addition) experiments for TP identification mentioned above were centrifuged at 4 °C, 12000 × *g* for 20 min, and the supernatant was loaded onto the Oasis HLB cartridge for solid phase extraction. TP identification was conducted by using the ultra-performance liquid chromatography system coupled to a hybrid quadrupole time-of-flight tandem mass spectrometer (UPLC-Q-TOF-MS/MS) (AB SCIEX, CA, USA) and Analyst TF 1.6 software (AB SCIEX, CA, USA).

The molecular formulae and predicted chemical structures of TPs were derived from the exact mass of $[M+H]^+$ or $[M-H]^-$ fragment ions and isotopic pattern. For suspect screening, a list of TPs was compiled considering previously reported TPs (Barr et al., 2012; Khunjar et al., 2011). Nontarget screening was further carried out to identify other possible TPs based on the following criteria: (1) mass accuracy tolerance < 5 ppm; (2) signal to noise ratio (S/N) > 100; (3) peak area > 10^5; (4) not detected in control group (inactivated cells); (5) TP-like changing pattern. Detailed TP identification procedure can be found in Supplementary Material.

Table 1
Target genes of RT-qPCR assays in this study.

Primer	Sequence (5′-3′)	Target gene	Amplicon size (bp)	Reference
amoAF	GGACTTCACGCTGTATCTG	*amoA*, encoding ammonia monooxygenase	135	(Yu and Chandran, 2010)
amoAR	GTGCCTTCTACAACGATTGG			
haoF	TGAGCCAGTCCAACGTGCAT	*hao*, encoding hydroxylamine oxidoreductase	85	
haoR	AAGGCAACAACCCTGCCTCA			
nirKF	TGCAGGGCATACTGGACGTT	*nirK*, encoding copper nitrite reductase	129	
nirKR	AGGTGAACGGGTGCGCATTT			
norBF	ACACAAATCACTGCCGCCCA	*norB*, encoding nitric oxide reductase subunit	200	
norBR	TGCAGTACACCGGCAAAGGT			
ncgAF	ACTCAGCATGCGATAGAGCC	*ncgA*, encoding multicopper oxidase	160	This study
ncgAR	TCGGGAGAGGATTCTTGGGT			
NE1543F	TCTGGCTGTATCACTCGCAC	NE1543, encoding multicopper oxidase	188	
NE1543R	TTTCAGGCCGCTTTCCTCAT			
EUBF	GTGSTGCAYGGYTGTCGTCA	16S rRNA gene	147	(Maeda et al., 2003)
EUBR	ACGTCRTCCMCACCTTCCTC			

2.5. EE2 cometabolic kinetics and modeling

Pre-grown culture was washed by fresh medium without ammonia and then resuspended with 200 μg/L EE2 (OD600 = 0.022) and separated into 150 mL vessels with gas permeable rubber stoppers. Groups 1–6 were set up with initial ammonia concentrations of 7, 14, 60, 120, 250, and 500 mg N/L, respectively (in duplicate). Other conditions were the same as batch tests mentioned above. Ammonia, nitrite and biomass were monitored every 6–12 h.

A reductant model including biomass growth, primary substrate utilization and cometabolic substrate transformation was used to describe the cometabolic kinetics of EE2 (Eqs. (1)–(3)) (Jesus et al., 2016).

Biomass growth:

$$\frac{dX}{dt} = Y\frac{k_{g,max}S_g}{K_{sg}+S_g}X - bX \quad (1)$$

Primary/growth substrate consumption:

$$\frac{dS_g}{dt} = -\frac{k_{g,max}S_g}{K_{sg}+S_g}X \quad (2)$$

Cometabolic substrate biotransformation:

$$\frac{dS_c}{dt} = -\frac{k_{c,max}S_c}{K_{sc}+S_c}\cdot\frac{S_g}{K_{sg}+S_g}X \quad (3)$$

where X is the biomass concentration (mg cell/L); S_g is the ammonia concentration (mg NH_4^+-N/L); $k_{g,max}$ is the maximum specific utilization rate of ammonia (mg N/mg cell·d); K_{sg} is the half-saturation coefficient for ammonia (mg N/L); S_c is the EE2 concentration (μg/L); $k_{c,max}$ is the maximum specific utilization rate of EE2 (μg/mg cell·d); K_{sc} is the half-saturation coefficient for EE2 (μg/L); Y is the biomass yield of AOB, 0.05 mg cell/mg N (Farges et al., 2012; Keen and Prosser, 1987); b is the first order decay coefficient of *N. europaea*, 0.0001 d^{-1}. T_c, the transformation capacity of EE2, i.e., the maximum amount of EE2 biotransformed per unit of ammonia consumed (μg EE2/mg N) is calculated by $T_c = k_{c,max}/k_{g,max}$ (Delgadillo-Mirquez et al., 2011; Fernandez-Fontaina et al., 2014). μ_{max}, the maximum specific growth rate of *N. europaea* (d^{-1}), is calculated by $\mu_{max} = k_{g,max}\cdot Y$.

Kinetic parameters $k_{g,max}$, K_{sg}, $k_{c,max}$, and K_{sc} were estimated simultaneously by fitting batch experimental data to the reductant model. Ordinary differential equations (ODE) were solved using the Runge-Kutta-Fehlberg method implemented in 1stOpt (http://www.7d-soft.com/en/), where weighted fitting was performed by minimizing the weighted sum of squared residuals (WSS) (Eq. (4)). μ_{max} and T_c were calculated accordingly. Estimated k_c values were plotted against EE2 and/or ammonia concentrations in Matlab.

$$WSS = \sum_{i=1}^{n}\left(\frac{(y_i - y_i')^2}{StdDev}\right) \quad (4)$$

where y is the estimated value; y' is the experimental value; n is the number of observations, and StdDev is the standard deviation.

2.6. RNA-seq and RT-qPCR

RNA was extracted and purified from 15 mL cell culture (t = 24 h in batch test) using RNeasy mini kit (Qiagen, USA) according to the manufacturer's instruction. RNA concentration and quality were assessed by

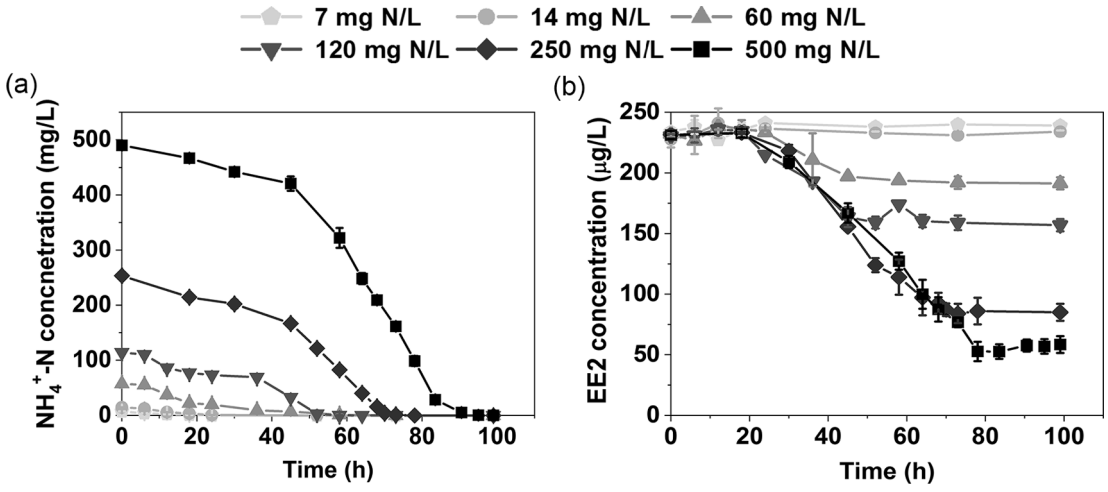

Fig. 1. Profiles of (a) ammonia and (b) EE2 at different initial NH_4^+-N concentrations. Error bars represent standard deviations of biological replicates.

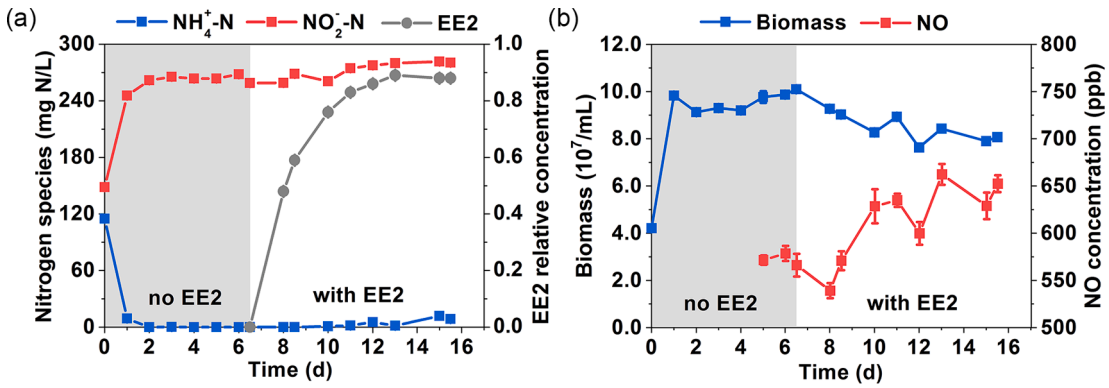

Fig. 2. Profiles of (a) NH_4^+-N, NO_2^--N and EE2; and (b) biomass and headspace NO in the chemostat. EE2 was added on day 6.5. EE2 relative concentration was calculated by C_e/C_i, where C_e and C_i represent EE2 concentrations in effluent and influent, respectively. Gray and white panels indicate phases before and after EE2 addition, respectively. Error bars represent standard deviations of biological triplicates.

using Colibri microvolume spectrometer (Titertek-Berthold, Germany). The whole RNA-Seq libraries were generated by using NEBNext® Ultra II™ Directional RNA Library Prep Kit for Illumina (New England Biolabs, USA). The library was paired-end sequenced on an Illumina Hiseq Xten platform (150 PE). Differentially expressed genes in batch cultures with and without EE2 were identified by the DEseq2 package in R 3.5.1, based on fragments per kilobase million (FPKMs) values of biological triplicates. Transcripts with adjusted *p* value (p_{adj}), i.e., FDR < 0.05 and $|\log_2$ (fold change)$|$ > 0.5 were considered as differentially expressed genes. Detailed data analysis procedure can be found in Supplementary Material.

RT-qPCR assays were used to validate selected differentially expressed genes identified by RNA-seq including *nirK*, *nirK* cluster gene *ncgA*, and NE1543, as well as other key genes involved in nitrogen metabolism, i.e., *amoA*, *hao*, and *norB* (Table 1). Genomic DNA removal and reverse transcription was performed using the PrimeScript RT reagent Kit with gDNA Eraser (TaKaRa, Japan) according to manufacturer's instruction. qPCR assays were performed in triplicate on a CFX Connect real-time PCR detection system (Bio-Rad, USA) with specific primer sets (Table 1). qPCR cycle included denaturing at 95℃ for 3 min followed by 40 cycles of 10 s at 95℃, 20 s at 55℃ and 10 s at 72℃.

3. Results

3.1. Cometabolic removal of EE2 by N. europaea

In batch test with heat-inactivated biomass, EE2 only decreased by <6% (Figure S1a). In the control group with EE2 but not ammonia, *N. europaea* did not grow (Figure S1b). Based on initial ammonia concentration, EE2 removal efficiency and rate varied dramatically from <1% to 76% and 0 to 13.9 ± 0.8 μg/mg cell·d, respectively (Fig. 1a, b). During the rapid removal of EE2, the rates of EE2 biotransformation and ammonia oxidation exhibited positive linear correlations (R^2 = 0.91–0.97, n = 6 for different groups, $p < 0.05$). However, at relatively low initial ammonia concentrations (7 and 14 mg N/L), no EE2 removal was observed. At concentrations equal to or above 60 mg N/L, there was a universal lag of EE2 removal varying from 18 h (>60 mg N/L) to 24 h (60 mg/L), and EE2 removal occurred afterwards. Additionally, no evident removal of EE2 was observed by adding hydroxylamine, an important intermediate of ammonia oxidation which could reacts with several ECs (Yu et al., 2018).

The uncoupled ammonia oxidation and EE2 removal was also found in the copper inhibition tests. Copper ions (Cu^{2+}) above 50 μg/L can be toxic to *N. europaea* (Dupont et al., 2011), and the uncoupling event was indeed observed at 50 μg/L Cu^{2+} (Figure S2), where ammonia oxidation slowed down during the first 24 h and EE2 removal completely ceased. Thereafter, with the gradual recovery of ammonia oxidation and reducing power supply, EE2 transformation resumed.

Table 2
Estimated kinetic parameters of EE2 cometabolism by *N. europaea* in this study.

Parameter	Description	Unit	Value
$k_{c,max}$	maximum specific removal rate of EE2	μg/mg cell·d	11.77 ± 1.79
K_{sc}	half-saturation coefficient for EE2	μg/L	69.97 ± 17.38
T_c	transformation capacity of EE2	μg EE2/mg N	1.01 ± 0.21
$k_{g,max}$	maximum specific consumption rate of ammonia	mg N/mg cell·d	11.41 ± 0.84
K_{sg}	half-saturation coefficient for ammonia	mg N/L	1.04 ± 0.94
μ_{max}	maximum specific growth rate	d^{-1}	0.59 ± 0.04

In the chemostat operated at steady state without EE2, ammonia was almost completely converted to nitrite (95 ± 1%). With 400 μg/L EE2 in the influent, an overall EE2 removal of 12 ± 1% and a specific removal rate of 2.1 ± 0.1 μg EE2/mg cell·d was achieved after 5 days. Meanwhile, ammonia-nitrite conversion gradually decreased to 90 ± 2% (Fig. 2a), and biomass reduced from (9.8 ± 0.3) × 10^7 cells/mL to (8.1 ± 0.1) × 10^7 cells/mL ($p < 0.05$, Fig. 2b). NO in the headspace of chemostat significantly increased by 12 ± 2% ($p < 0.01$) from 572 ± 6 ppb to 648 ± 17 ppb upon EE2 addition. N_2O emission did not change significantly (120–150 ppb, Figure S3).

3.2. Kinetics of EE2 cometabolism

The six kinetic parameters estimated based on the reductant model are listed in Table 2. The maximum EE2 specific removal rate ($k_{c,max}$) represented the potential of EE2 cometabolism by *N. europaea* with unlimited ammonia concentrations (Fig. 3a). The specific removal rate of EE2 (k_c) varied upon ammonia and EE2 concentrations (Fig. 3b), and was more sensitive to the latter. Figure S4 showed the estimated and the measured ammonia (S_g), EE2 (S_c) and biomass (X) concentrations in selected batch experiments.

3.3. Transformation products of EE2

At least nine TPs were identified in our batch and chemostat experiments (Table 3). M294 ($C_{20}H_{22}O_2$ with two proposed structures), M310 ($C_{20}H_{22}O_3$), M312 ($C_{20}H_{24}O_3$) and M314 ($C_{20}H_{26}O_3$) were newly reported TPs in this study, and detected only in the positive mode ($[M+H]^+$, individual MS and MS/MS spectra shown in Figure S5). Herein, M312 was not OH-EE2 but its possible tautomer via keto-enol tautomerism where ketone and enol can be interconverted (Ngundi et al.,

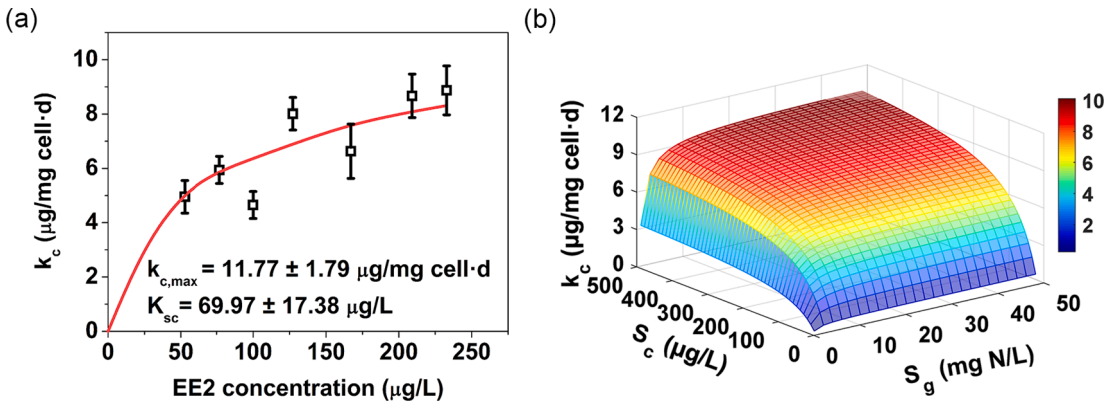

Fig. 3. (a) Specific removal rate of EE2 (k_c) as a function of EE2 concentration with unlimited ammonia. Squares are the experimental data, and the red curve represents reductant model fitting results. Error bars represent standard deviations of biological replicates. (b) 3D plot of EE2 specific removal rate (k_c) varying upon ammonia (S_g) and EE2 (S_c) concentrations. Color bar indicates the range of k_c. (For interpretation of the references to color in this figure legend, the reader is referred to the web version of this article.)

Table 3
The main EE2 transformation products identified in this study.

Compound	Molecular formula	Proposed structure	Reference
M296 (EE2)	$C_{20}H_{24}O_2$	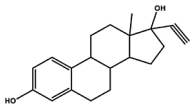	
M294	$C_{20}H_{22}O_2$ (–2H)	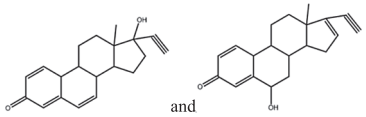	This study
M310	$C_{20}H_{22}O_3$ (+O, –2H)	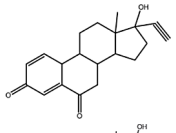	This study
M312	$C_{20}H_{24}O_3$ (+O)	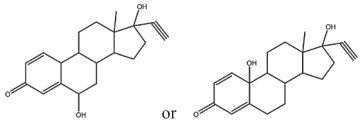	This study and (Della Greca et al., 2008)
M314	$C_{20}H_{26}O_3$ (+O, +2H)	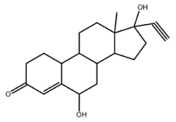	This study
M376 (sulfo-EE2)	$C_{20}H_{24}O_5S$ (+S, +3O)	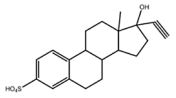	(Khunjar et al., 2011; Yi and Harper, 2007)
M341 (nitro-EE2)	$C_{20}H_{23}O_4N$ (+2O, +N, -H)	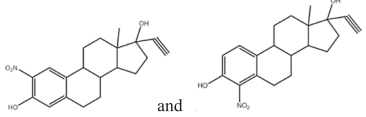	(Gaulke et al., 2008; Skotnicka-Pitak et al., 2009)
M386 (dinitro-EE2)	$C_{20}H_{22}O_6N_2$ (+4O, +2N, –2H)	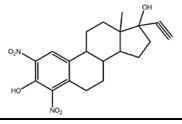	(Gaulke et al., 2008)

2003), because it only responded to the $[M + H]^+$ mode, indicating a structure without phenyl group. Therefore, this study suggested another possible structure of the initial product instead of OH-EE2. The other TPs were potentially derived from M312 via dehydration and redox reactions. MS-peak extracted ion chromatograms of the biotic TPs and proposed biotransformation pathways can be found in Supplementary Material (Figure S6, S7). Previously reported TPs of EE2, including nitro-EE2 (M341, with two proposed structures), dinitro-EE2 (M386), and sulfo-EE2 (M376) were also found in this study. Batch and chemostat operations resulted in slightly different TPs, and more details were described in Table S1.

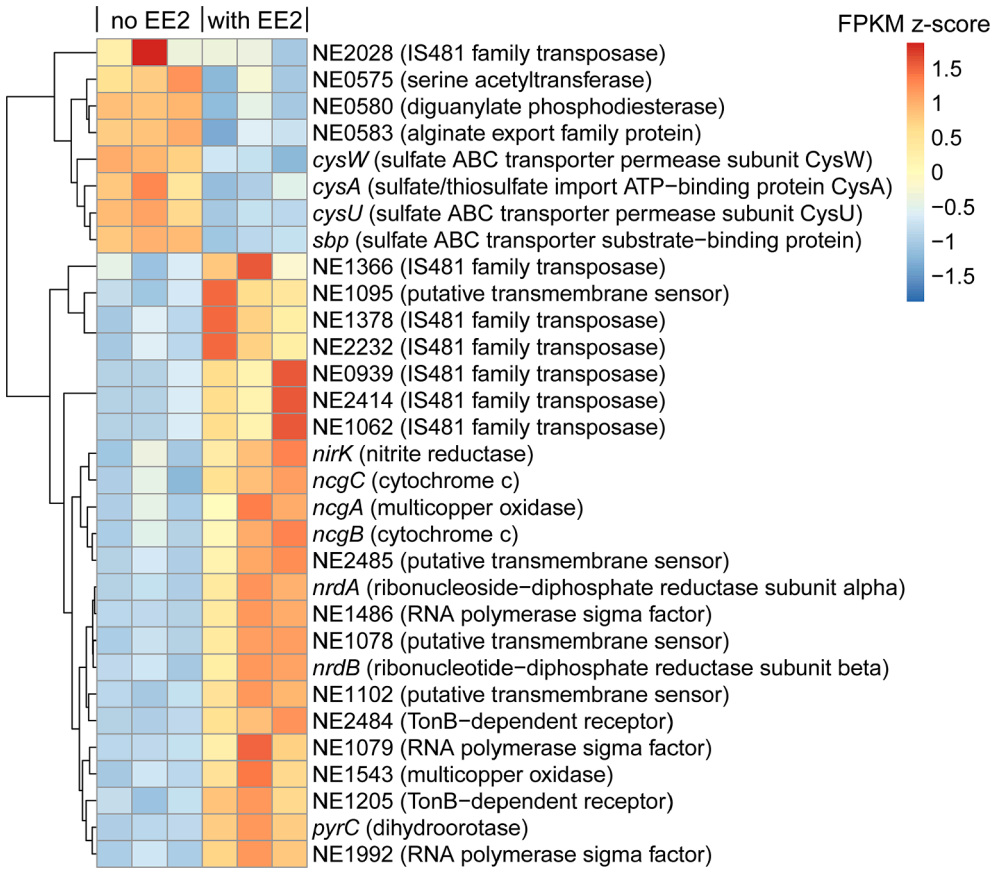

Fig. 4. Heat map of differentially expressed genes (rows) between samples (columns) with and without EE2 in batch experiment ($|\log_2$ fold change$| > 0.5$, FDR < 0.05). Color bar represents the row z-score of fragments per kilobase per million reads mapped (FPKM). Orange, up-regulation; blue, down-regulation. (For interpretation of the references to color in this figure legend, the reader is referred to the web version of this article.)

3.4. Differentially expressed genes during EE2 biotransformation

RNA-seq revealed thirty-four differentially expressed genes during EE2 cometabolism (Fig. 4 and Figure S8), broadly involved in electron transfer, energy metabolism, transcriptional regulation, and substrate transport. Among them, *nirK* cluster genes (*ncgABC* and *nirK*) increased significantly by 1.42-, 1.44-, 1.45-, and 1.47-fold (FDR < 0.05), respectively. They are mainly involved in nitrite reduction to NO in *N. europaea* (Cantera and Stein, 2007). *ncgB* and *ncgC* encode two cytochromes with unknown functions, and *ncgA* encodes a well characterized two-domain multicopper oxidase, NcgA (Beaumont et al., 2005; Lawton et al., 2013). A distant gene NE1543 was also up-regulated during EE2 cometabolism (by 1.68-fold, FDR < 0.05), encoding another multicopper oxidase with unknown function. The upregulations of *nirK*, *ncgA*, and NE1543 were verified by RT-qPCR assays in chemostat experiments, where they increased by up to 2.17-, 3.97-, and 6.71-fold during EE2 cometabolism, respectively ($p < 0.05$) (Fig. 5a–c). Down-regulated genes (by 1.58- to 2.0-fold, FDR < 0.05) were mainly involved in sulfur transport and metabolism, including *sbp*, *cysU*, *cysW*, *cysA* (encoding sulfate transporter CysATWP-Sbp) and NE0575 (encoding serine acetyltransferase).

Although *amoA* might be involved in the initiation of EE2 transformation, evidenced by the formation of mono-hydroxylated TPs, it was not differentially expressed between "no EE2" and "with EE2" groups. In the RT-qPCR assays, *amoA* expression even decreased by nearly 40% on day 5 after the addition of EE2 in the chemostat (Fig. 5d). The expression of the other two nitrogen metabolism genes, *hao* and *norB* were unaffected by EE2 (Fig. 5e, 5f).

4. Discussion

4.1. Reducing power availability determines the relationship between EE2 cometabolism and ammonia oxidation

In this study, biotransformation was the dominant process contributing to EE2 removal by *N. europaea*, while adsorption and hydroxylamine-mediated abiotic transformation were minimal (Forrez et al., 2009; Khunjar et al., 2008). Additionally, EE2 could not support the growth of *N. europaea* as the sole energy source, i.e., ammonia was required for the initiation of EE2 biotransformation. The "coupling" relationship ("C", Fig. 6) between primary metabolism and cometabolism occurred when initial ammonia concentration was in the range of 38–180 mg N/L, where the production and consumption of reductants were similar, leading to widely reported positive correlations (Jantanaprasartporn et al., 2018; Yi and Harper, 2007).

The most interesting finding from the batch experiments was that ammonia oxidation and EE2 removal did not always exhibit positive linear relationship. The first uncoupling event occurred during the "activation" phase ("A", Fig. 6) within 0–38 mg N/L of ammonia, where ammonia was oxidized but EE2 removal was not initiated. Notably, this represents the typical concentration of ammonia at WWTPs (Sun et al., 2016; Zhang et al., 2016). A similar adaptation phase in EC removal was also observed elsewhere (De Wever et al., 2007; Hamon et al., 2018). The cometabolism of non-growth substrate EE2 was expected to consume the reducing power generated from ammonia oxidation (Barr et al., 2012; Jantanaprasartporn et al., 2018; Jesus et al., 2016), and our study further proved that sufficient reducing power was required to initiate cometabolism. Quantitatively, based on batch experiments, the "activation" of EE2 cometabolic removal required an oxidation of 38.1

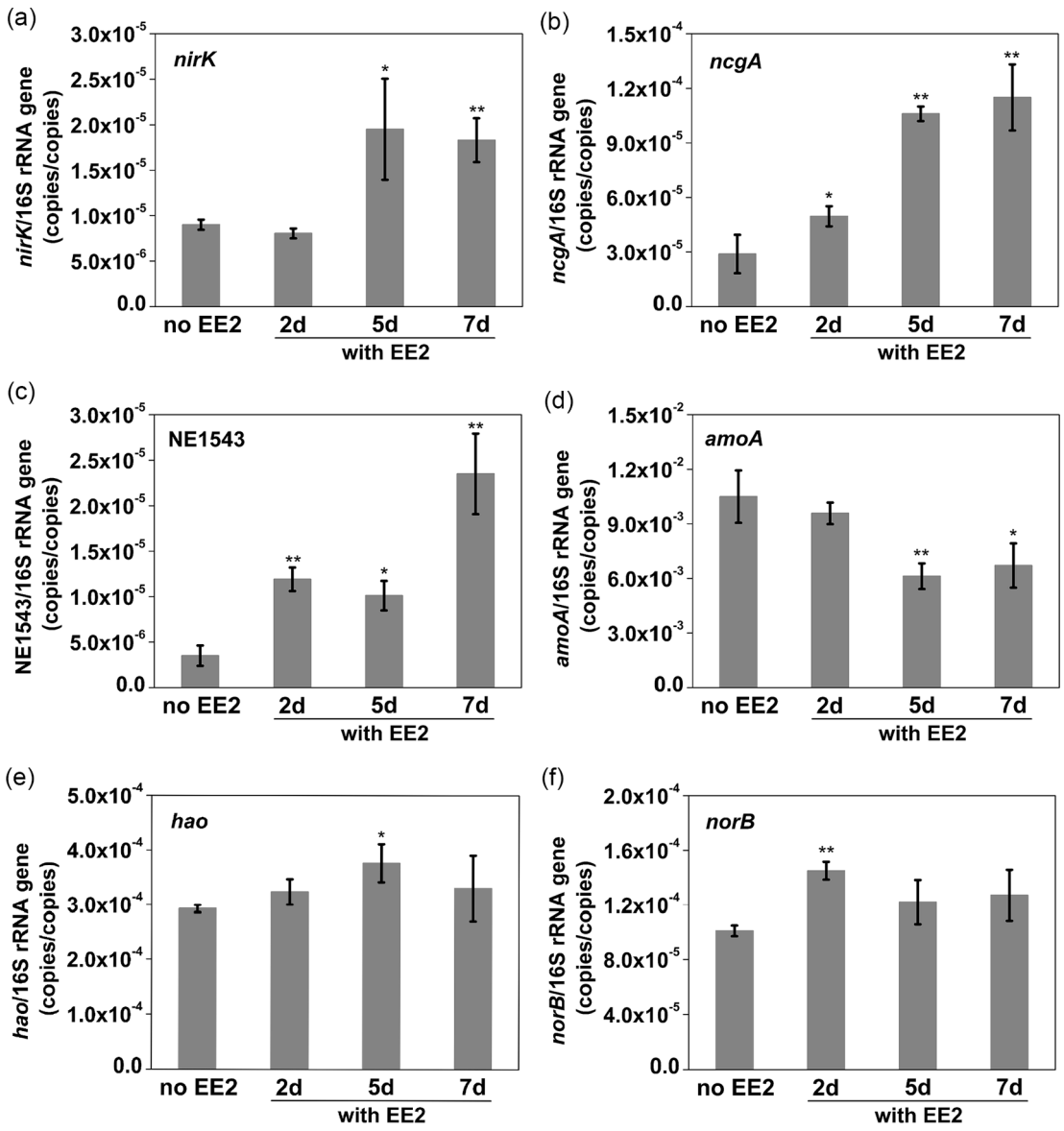

Fig. 5. Gene expression levels of (a) *nirK*, (b) *ncgA*, (c) NE1543, (d) *amoA*, (e) *hao* and (f) *norB* before and after EE2 addition in the chemostat. Error bars represent standard deviations of biological triplicates. Statistically significant differences compared with "no EE2" were indicated by * $p < 0.05$, ** $p < 0.01$.

± 2.5 mg NH_4^+-N/L, and the reducing power generated was 0.95 ± 0.06 mol NADH/L according to the stoichiometry of the electron transport chain (NADH formed: ammonia oxidized = 0.35:1 in AOB) (Soliman and Eldyasti, 2018). Primary metabolism and cometabolism were again uncoupled in the "saturation" cometabolism phase ("S", Fig. 6) with initial ammonia above 180 mg N/L, where increasing initial ammonia concentration would not further enhance EE2 removal. In the "saturation" phase, there could be an oversupply of reducing power required for EE2 cometabolism. The complex relationships between cometabolism and primary metabolism should be carefully examined to remove mixed traditional pollutants and ECs (e.g., ammonia and EE2) at WWTPs.

4.2. Estimated kinetics of EE2 cometabolism

As ammonia concentrations in all batch experiments, from beginning to the end, were typically higher than half-saturation coefficient for ammonia (K_{sg}), the biotransformation kinetics of EE2 was more prone to the EE2 concentration due to cell's lower affinity to EE2. Nevertheless, ammonia concentrations in real wastewater nitrifying reactors can be as low as 1.5–5.0 mg N/L (Sun et al., 2016; Zhang et al., 2016), where ammonia could also be a rate-limiting factor for EE2 transformation. The estimated T_c was higher than those of other ECs by highly enriched nitrifying activated sludge (0.08–0.56 μg/mg N) (Fernandez-Fontaina et al., 2014), suggesting relatively high cometabolic potential of *N. europaea* cells towards EE2. The maximum specific growth rate (μ_{max}), ammonia specific consumption rate ($k_{g,max}$) and K_{sg} were similar to previously reported values (Blackburne et al., 2007; Keen and Prosser, 1987; Maestre et al., 2013), again indicating insignificant influence of EE2 cometabolism on bacterial growth in short term. In this study, batch tests performed better than chemostat in terms of overall EE2 removal, as ammonia was limited in the latter (typically <1 mg N/L), probably resulting in insufficient energy supply for EE2 transformation. Additionally, the difference between TPs in batch and chemostat experiments was possibly due to the different physiological status of *N. europaea* cells under the two growth conditions and the resulting differential regulations of both primary metabolism and EE2 cometabolism. Similar observation was reported in a previous study (Skotnicka-Pitak et al., 2009).

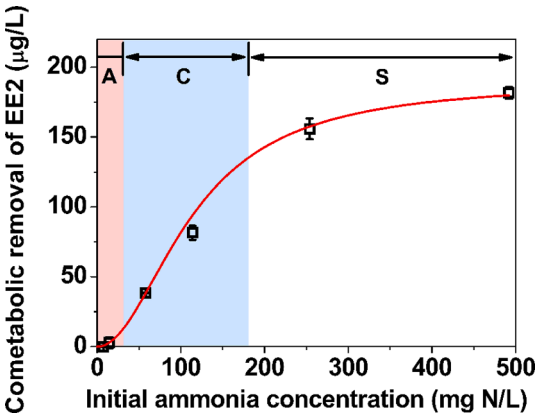

Fig. 6. Non-linear relationship between initial ammonia concentration and EE2 removal by unacclimated *N. europaea*. The three phases of relationship include: "activation (A)" of EE2 cometabolism (light red, 0–38 mg N/L); "coupling (C)" ammonia oxidation and EE2 cometabolism (light blue, 38–180 mg N/L); "saturation (S)" of EE2 cometabolism (white, >180 mg N/L). Data were collected from batch experiments (G1−G6) and fitted to a Logistics-like model. Error bars represent standard deviations of biological replicates. (For interpretation of the references to color in this figure legend, the reader is referred to the web version of this article.)

4.3. Nitric oxide formation was elevated during EE2 cometabolism

The elevated NO formation during EE2 cometabolism in the chemostat is noteworthy. As an essential intermediate in ammonia oxidation, NO has long been considered as a product of nitrifier denitrification (from nitrite to NO and N_2O) catalyzed by NirK (Horrell et al., 2017; Lawton et al., 2013). More recently, it was identified as the obligate nitrification intermediate as the direct product of hydroxylamine oxidation by HAO (Caranto and Lancaster, 2017). Therefore, NO can be generated by *N. europaea* via HAO-mediated oxidation pathway, or NirK-mediated reduction pathway (Kits et al., 2019). EE2 cometabolism stimulated either or both of the pathways, leading to elevated NO formation.

NO is an important precursor of reactive nitrogen species (RNS), a non-specific potent oxidative agent damaging cell compounds including enzymes, lipids and DNA (Porrini et al., 2020). Its accumulation during the long-term exposure to EE2 potentially contributed to the biomass inhibition observed in the chemostat experiment. However, the inhibitory effects of EE2 were not observed during short-term batch tests in a previous study (Khunjar et al., 2008), which may be due to different EE2 exposure time and cell physiological status between batch and chemostat. NO can abiotically react with superoxide to form a strong toxic oxidant peroxynitrite ($ONOO^-$) (Koppenol, 1994), which could subsequently react with phenolic compounds (Ramezanian et al., 1996), leading to the formation of nitro-EE2 (M341) and dinitro-EE2 (M386). These two compounds, however, were previously regarded as abiotic transformation products of EE2 via nitrite-mediated nitration (Gaulke et al., 2008). Biotic nitration of EE2 was also possible, because cytochromes P450 can utilize O_2 and NO to nitrate aromatic compounds (Louka et al., 2020). NO is also a trace gas in atmosphere that can form photochemical smog, acid rain and haze (Heil et al., 2016; Hong et al., 2017). In this study, NO emitted during EE2 cometabolism was much higher than its atmospheric level (typically below 100 ppb) (Baraldi et al., 1998; Corradi et al., 1998; Miyazaki et al., 2008), raising concerns on the potential air pollution caused by the cometabolism of EE2 and other ECs at WWTPs.

4.4. nirK cluster genes were up-regulated during EE2 cometabolism

nirK cluster genes were significantly up-regulated during EE2 cometabolism. They function in the nitrifier denitrification process to detoxify nitrite and NO (Beaumont et al., 2005; Sedlacek et al., 2020). There were two possible explanations for the up-regulated *nirK* cluster genes and NE1543 in both batch and chemostat operations: as stress response genes to EE2 and/or participating in EE2 metabolism. The latter was conceivable because: 1) we found that *nirK* and *ncgA* upregulations coincided with EE2 transformation rather than EE2 exposure (Figure S9); 2) multicopper oxidases could function in oxidoreduction and electron transfer (Kaur et al., 2019; Nishide et al., 2020; Shraddha et al., 2011); 3) the overexpression of *nirK* favored electron flux toward reductant generation thus potentially facilitated EE2 biotransformation (Starkenburg et al., 2008).

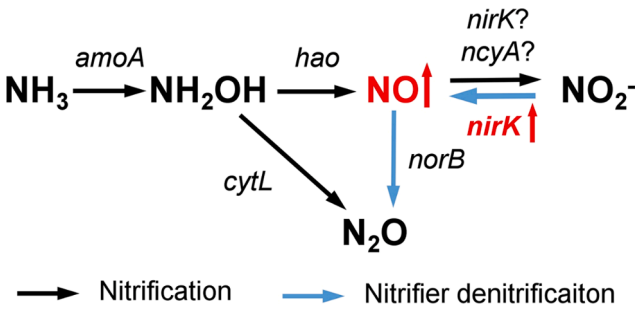

Fig. 7. Genes involved in the nitrification and nitrifier denitrification pathways in *N. europaea*. Red arrows stand for upregulated genes or accumulated products during EE2 cometabolism, and unchanged genes are denoted in black. *amoA*, encoding ammonia monooxygenase; *hao*, encoding hydroxylamine oxidoreductase; *ncyA*, encoding red copper protein nitrosocyanin; *nirK*, encoding copper nitrite reductase; *norB*, encoding nitric oxide reductase; *cytL*, encoding cytochrome P460. (For interpretation of the references to color in this figure legend, the reader is referred to the web version of this article.)

The roles of NirK in bacterial and archaeal nitrification remain controversial. Traditionally, it is believed that NirK in AOB catalyzes the one electron reduction of nitrite to NO. Other functions were also reported, such as facilitating ammonia oxidation and intracellular redox-balance (Cantera and Stein, 2007; Starkenburg et al., 2008). Recently, a new role of NirK as a candidate NO oxidoreductase (NOO) has been proposed (Caranto and Lancaster, 2017; Wijma et al., 2004) (Fig. 7), but this reversible process of nitrifier denitrification is kinetically unfavorable (Kits et al., 2019). These studies, together with the results obtained from this study (simultaneous upregulations of *nirK* cluster genes and elevated NO emission) generally supported a more critical role of NirK in nitrifier denitrification. Future efforts on unraveling the roles of NirK in EE2 cometabolism, or cometabolism of broader ECs, would be of help to understanding the functions of NirK in AOB as well.

5. Conclusions

This study revealed a previously overlooked complex relationship between primary metabolism (ammonia oxidation) and EE2 cometabolism by nitrifying bacteria. Traditionally, it is believed that increasing ammonia concentration would enhance EE2 cometabolism, but our findings indicate that this is valid when the two are in a "coupling" relationship. When the reducing power is under- (during "activation" phase) or over-supplied (during "saturation" phase), EE2 cometabolism can be uncoupled from ammonia oxidation. It is worth noting that the initial ammonia concentration in the "activation" phase is among the typical range of municipal wastewater, and thus insufficient reducing power supply may hinder EE2 cometabolism. Interrupted reductant supply and/or electron transfer caused by environmental stresses (e.g., copper ions in this study) would also hamper this process in natural and engineered biosystems. Therefore, the addition of alternative energy sources and stabilizing reducing power supply would benefit cometabolic EE2 removal.

Previous work primarily focused on the greenhouse gas N_2O formation during nitrification, but our finding highlighted the necessity of

paying attention to the elevated NO formation during EE2 cometabolism and its toxicity in aqueous phase. Whether the cometabolism of other ECs by AOB would also lead to elevated NO or N_2O formation should be addressed in future studies. Additionally, we demonstrated for the first time that *nirK* cluster genes associated mainly with nitrifier denitrification pathway were up-regulated during EE2 cometabolism. The highly expressed *nirK* and multicopper oxidase genes were potentially stress responses to chronic EE2 exposure or involved in the cometabolic biotransformation of EE2. Genetic engineering would be helpful to further verify the roles of these up-regulated genes, but as they may be essential to the fundamental biological processes of AOB, this represents a challenging task. The fate, toxicity and stability of diverse TPs deserve detailed investigations, too. These findings and proposed research tasks would expend our knowledge on the kinetics, TPs and molecular mechanism of EE2 cometabolism by AOB, which is critical for the design and operation of biological wastewater treatment processes towards enhanced removal of both traditional pollutants and ECs.

Declaration of Competing Interest

The authors declare that they have no known competing financial interests or personal relationships that could have appeared to influence the work reported in this paper.

Acknowledgement

This work was supported by the National Key Research and Development Program of China (2019YFC0408800), the National Natural Science Foundation of China (21836003), and the Fundamental Research Funds for the Central Universities (2020FZZX001-06). We are grateful to Wenbo Chai and Shaoyi Xu for critical and valuable discussions. We thank Weiwei Shen and Jie Wang for technical support.

Appendix A. Supplementary material

Supplementary data to this article can be found online at https://doi.org/10.1016/j.envint.2021.106528.

References

Adeel, M., Song, X., Wang, Y., Francis, D., Yang, Y., 2017. Environmental impact of estrogens on human, animal and plant life: A critical review. Environ. Int. 99, 107–119. https://doi.org/10.1016/j.envint.2016.12.010.

Baraldi, E., Azzolin, N.M., Dario, C., Carra, S., Ongaro, R., Biban, P., Zacchello, F., 1998. Effect of atmospheric nitric oxide (NO) on measurements of exhaled NO in asthmatic children. Pediatr. Pulmonol. 26, 30–34. https://doi.org/10.1002/(SICI)1099-0496(199807)26:1<30::AID-PPUL6>3.0.CO;2-M.

Barr, W.J., Yi, T., Aga, D., Acevedo, O., Harper, W.F., 2012. Using electronic theory to identify metabolites present in 17alpha-ethinylestradiol biotransformation pathways. Environ. Sci. Technol. 46, 760–768. https://doi.org/10.1021/es201774r.

Beaumont, H.J.E., Lens, S.I., Westerhoff, H.V., van Spanning, R.J.M., 2005. Novel *nirK* cluster genes in *Nitrosomonas europaea* are required for NirK-dependent tolerance to nitrite. J. Bacteriol. 187, 6849–6851. https://doi.org/10.1128/jb.187.19.6849-6851.2005.

Blackburne, R., Vadivelu, V.M., Yuan, Z., Keller, J., 2007. Determination of growth rate and yield of nitrifying bacteria by measuring carbon dioxide uptake rate. Water Environ. Res. 79, 2437–2445. https://doi.org/10.2175/106143007x212139.

Caldwell, D.J., Mastrocco, F., Anderson, P.D., Lange, R., Sumpter, J.P., 2012. Predicted-no-effect concentrations for the steroid estrogens estrone, 17beta-estradiol, estriol, and 17alpha-ethinylestradiol. Environ. Toxicol. Chem. 31, 1396–1406. https://doi.org/10.1002/etc.1825.

Cantera, J.J.L., Stein, L.Y., 2007. Role of nitrite reductase in the ammonia-oxidizing pathway of *Nitrosomonas europaea*. Arch. Microbiol. 188, 349–354. https://doi.org/10.1007/s00203-007-0255-4.

Caranto, J.D., Lancaster, K.M., 2017. Nitric oxide is an obligate bacterial nitrification intermediate produced by hydroxylamine oxidoreductase. Proc. Natl. Acad. Sci. U. S. A. 114, 8217–8222. https://doi.org/10.1073/pnas.1704504114.

China, SEPA, 2002. Water and wastewater monitoring and analysis methods (4th Edition). China Environment Science Press, Beijing.

Corradi, M., Pelizzoni, A., Majori, M., Cuomo, A., de' Munari, E., Pesci, A., 1998. Influence of atmospheric nitric oxide concentration on the measurement of nitric oxide in exhaled air. Thorax 53, 673–676. https://doi.org/10.1136/thx.53.8.673.

De Wever, H., Weiss, S., Reemtsma, T., Vereecken, J., Muller, J., Knepper, T., Rorden, O., Gonzalez, S., Barcelo, D., Dolores Hernando, M., 2007. Comparison of sulfonated and other micropollutants removal in membrane bioreactor and conventional wastewater treatment. Water Res. 41, 935–945. https://doi.org/10.1016/j.watres.2006.11.013.

Delgadillo-Mirquez, L., Lardon, L., Steyer, J.P., Patureau, D., 2011. A new dynamic model for bioavailability and cometabolism of micropollutants during anaerobic digestion. Water Res. 45, 4511–4521. https://doi.org/10.1016/j.watres.2011.05.047.

Della Greca, M., Pinto, G., Pistillo, P., Pollio, A., Previtera, L., Temussi, F., 2008. Biotransformation of ethinylestradiol by microalgae. Chemosphere 70 (11), 2047–2053. https://doi.org/10.1016/j.chemosphere.2007.09.011.

Dupont, C.L., Grass, G., Rensing, C., 2011. Copper toxicity and the origin of bacterial resistance—new insights and applications. Metallomics 3, 1109–11018. https://doi.org/10.1039/c1mt00107h.

Farges, B., Poughon, L., Roriz, D., Creuly, C., Dussap, C.G., Lasseur, C., 2012. Axenic cultures of *Nitrosomonas europaea* and *Nitrobacter winogradskyi* in autotrophic conditions: a new protocol for kinetic studies. Appl. Biochem. Biotechnol. 167, 1076–1091. https://doi.org/10.1007/s12010-012-9651-6.

Fernandez-Fontaina, E., Carballa, M., Omil, F., Lema, J.M., 2014. Modelling cometabolic biotransformation of organic micropollutants in nitrifying reactors. Water Res. 65, 371–383. https://doi.org/10.1016/j.watres.2014.07.048.

Forrez, I., Carballa, M., Boon, N., Verstraete, W., 2009. Biological removal of 17α-ethinylestradiol (EE2) in an aerated nitrifying fixed bed reactor during ammonium starvation. J. Chem. Technol. Biotechnol. 84, 119–125. https://doi.org/10.1002/jctb.2016.

Gaulke, L.S., Strand, S.E., Kalhorn, T.F., Stensel, H.D., 2008. 17α-ethinylestradiol transformation via abiotic nitration in the presence of ammonia oxidizing bacteria. Environ. Sci. Technol. 42, 7622–7627. https://doi.org/10.1021/es801503u.

Gavrilescu, M., Demnerova, K., Aamand, J., Agathos, S., Fava, F., 2015. Emerging pollutants in the environment: present and future challenges in biomonitoring, ecological risks and bioremediation. N. Biotechnol. 32, 147–156. https://doi.org/10.1016/j.nbt.2014.01.001.

Gusseme, D., Bart, Pycke, B., Hennebel, T., Marcoen, A., Vlaeminck, S.E., Noppe, H., Boon, N., Verstraete, W., 2009. Biological removal of 17α-ethinylestradiol by a nitrifier enrichment culture in a membrane bioreactor. Water Res. 43, 2493–2503. https://doi.org/10.1016/j.watres.2009.02.028.

Hamid, H., Eskicioglu, C., 2012. Fate of estrogenic hormones in wastewater and sludge treatment: A review of properties and analytical detection techniques in sludge matrix. Water Res. 46, 5813–5833. https://doi.org/10.1016/j.watres.2012.08.002.

Hamon, P., Moulin, P., Ercolei, L., Marrot, B., 2018. Performance of a biomass adapted to oncological ward wastewater vs. biomass from municipal WWTP on the removal of pharmaceutical molecules. Water Res. 128, 193–205. https://doi.org/10.1016/j.watres.2017.10.037.

Heil, J., Vereecken, H., Brüggemann, N., 2016. A review of chemical reactions of nitrification intermediates and their role in nitrogen cycling and nitrogen trace gas formation in soil. Eur. J. Soil Sci. 67, 23–39. https://doi.org/10.1111/ejss.12306.

Hong, Z., Wang, Z., Li, X., 2017. Catalytic oxidation of nitric oxide (NO) over different catalysts: an overview. Catal. Sci. Technol. 7, 3440–3452. https://doi.org/10.1039/c7cy00760d.

Horrell, S., Kekilli, D., Strange, R.W., Hough, M.A., 2017. Recent structural insights into the function of copper nitrite reductases. Metallomics 9, 1470–1482. https://doi.org/10.1039/c7mt00146k.

Jantanaprasartporn, A., Maneerat, S., Rongsayamanont, C., 2018. Importance of culture history on 17α-ethinylestradiol cometabolism by nitrifying sludge. Environ. Res. Eng. Manag. 23, 28–35. https://doi.org/10.4491/eer.2017.044.

Jesus, J., Frascari, D., Pozdniakova, T., Danko, A.S., 2016. Kinetics of aerobic cometabolic biodegradation of chlorinated and brominated aliphatic hydrocarbons: A review. J. Hazard Mater. 309, 37–52. https://doi.org/10.1016/j.jhazmat.2016.01.065.

Kaur, K., Sharma, A., Capalash, N., Sharma, P., 2019. Multicopper oxidases: Biocatalysts in microbial pathogenesis and stress management. Microbiol. Res. 222, 1–13. https://doi.org/10.1016/j.micres.2019.02.007.

Keen, G.A., Prosser, J.I., 1987. Steady state and transient growth of autotrophic nitrifying bacteria. Arch. Microbiol. 147, 73–79. https://doi.org/10.1007/BF00492908.

Khunjar, W.O., Mackintosh, S.A., Skotnicka-Pitak, J., Baik, S., Aga, D.S., Love, N.G., 2011. Elucidating the relative roles of ammonia oxidizing and heterotrophic bacteria during the biotransformation of 17alpha-ethinylestradiol and trimethoprim. Environ. Sci. Technol. 45, 3605–3612. https://doi.org/10.1021/es1037035.

Khunjar, W.O., Skotnicka-Pitak, J., Love, N.G., Aga, D., Harper, J.W.F., 2008. Biotransformation of pharmaceuticals and personal care products (PPCPs) during nitrification: the role of ammonia oxidizing bacteria versus heterotrophic bacteria. In: World Environmental and Water Resources Congress 2008.

Kits, K.D., Jung, M.Y., Vierheilig, J., Pjevac, P., Sedlacek, C.J., Liu, S., Herbold, C., Stein, L.Y., Richter, A., Wissel, H., Bruggemann, N., Wagner, M., Daims, H., 2019. Low yield and abiotic origin of N_2O formed by the complete nitrifier *Nitrospira inopinata*. Nat. Commun. 10, 1836. https://doi.org/10.1038/s41467-019-09790-x.

Koppenol, W.H., 1994. NO comments. Nature 367, 28. https://doi.org/10.1038/367028b0.

Laurenson, J.P., Bloom, R.A., Page, S., Sadrieh, N., 2014. Ethinyl estradiol and other human pharmaceutical estrogens in the aquatic environment: a review of recent risk assessment data. AAPS J. 16, 299–310. https://doi.org/10.1208/s12248-014-9561-3.

Lawton, T.J., Bowen, K.E., Sayavedra-Soto, L.A., Arp, D.J., Rosenzweig, A.C., 2013. Characterization of a nitrite reductase involved in nitrifier denitrification. J. Biol. Chem. 288, 25575–25583. https://doi.org/10.1074/jbc.M113.484543.

Lima, D.L., Silva, C.P., Otero, M., Esteves, V.I., 2013. Low cost methodology for estrogens monitoring in water samples using dispersive liquid-liquid microextraction and

HPLC with fluorescence detection. Talanta 115, 980–985. https://doi.org/10.1016/j.talanta.2013.07.007.
Liu, L., Binning, P.J., Smets, B.F., 2015. Evaluating alternate biokinetic models for trace pollutant cometabolism. Environ. Sci. Technol. 49, 2230–2236. https://doi.org/10.1021/es5035393.
Louka, S., Barry, S.M., Heyes, D.J., Mubarak, M.Q.E., Ali, H.S., Alkhalaf, L.M., Munro, A. W., Scrutton, N.S., Challis, G.L., de Visser, S.P., 2020. Catalytic mechanism of aromatic nitration by cytochrome P450 TxtE: involvement of a ferric-peroxynitrite intermediate. J. Am. Chem. Soc. 142, 15764–15779. https://doi.org/10.1021/jacs.0c05070.
Luo, Y., Guo, W., Ngo, H.H., Nghiem, L.D., Hai, F.I., Zhang, J., Liang, S., Wang, X.C., 2014. A review on the occurrence of micropollutants in the aquatic environment and their fate and removal during wastewater treatment. Sci. Total Environ. 473–474, 619–641. https://doi.org/10.1016/j.scitotenv.2013.12.065.
Maeda, H., Fujimoto, C., Haruki, Y., Maeda, T., Kokeguchi, S., Petelin, M., Arai, H., Tanimoto, I., Nishimura, F., Takashiba, S., 2003. Quantitative real-time PCR using TaqMan and SYBR Green for *Actinobacillus actinomycetemcomitans*, *Porphyromonas gingivalis*, *Prevotella intermedia*, tetQ gene and total bacteria. FEMS Immunol. Med. Microbiol. 39 (1), 81–86. https://doi.org/10.1016/s0928-8244(03)00224-4.
Maestre, J.P., Wahman, D.G., Speitel Jr., G.E., 2013. Monochloramine cometabolism by *Nitrosomonas europaea* under drinking water conditions. Water Res. 47, 4701–4709. https://doi.org/10.1016/j.watres.2013.05.019.
Men, Y., Achermann, S., Helbling, D.E., Johnson, D.R., Fenner, K., 2017. Relative contribution of ammonia oxidizing bacteria and other members of nitrifying activated sludge communities to micropollutant biotransformation. Water Res. 109, 217–226. https://doi.org/10.1016/j.watres.2016.11.048.
Miyazaki, K., Matsumoto, J., Kato, S., Kajii, Y., 2008. Development of atmospheric NO analyzer by using a laser-induced fluorescence NO_2 detector. Atmospheric Environ. 42, 7812–7820. https://doi.org/10.1016/j.atmosenv.2008.05.056.
Ngundi, M.M., Sadik, O.A., Yamaguchi, T., Suye, S.-I., 2003. First comparative reaction mechanisms of β-estradiol and selected environmental hormones in a redox environment. Electrochem. commun. 5, 61–67. https://doi.org/10.1016/S1388-2481(02)00538-6.
Nguyen, P.Y., Carvalho, G., Reis, M.A.M., Oehmen, A., 2020. A review of the biotransformations of priority pharmaceuticals in biological wastewater treatment processes. Water Res. 188, 116446 https://doi.org/10.1016/j.watres.2020.116446.
Nishide, Y., Kageyama, D., Hatakeyama, M., Yokoi, K., Jouraku, A., Tanaka, H., Koga, R., Futahashi, R., Fukatsu, T., 2020. Diversity and function of multicopper oxidase genes in the stinkbug Plautia stali. Sci. Rep. 10, 3464. https://doi.org/10.1038/s41598-020-60340-8.
Pauwels, B., Noppe, H., De Brabander, H., Verstraete, W., 2008. Comparison of steroid hormone concentrations in domestic and hospital wastewater treatment plants. J. Environ. Eng. (New York) 134, 933–936. https://doi.org/10.1061/(ASCE)0733-9372(2008)134:11(933).
Petrie, B., Barden, R., Kasprzyk-Hordern, B., 2015. A review on emerging contaminants in wastewaters and the environment: current knowledge, understudied areas and recommendations for future monitoring. Water Res. 72, 3–27. https://doi.org/10.1016/j.watres.2014.08.053.
Porrini, C., Ramarao, N., Tran, S.L., 2020. Dr. NO and Mr. Toxic – the versatile role of nitric oxide. Biol. Chem. 401, 547–572. https://doi.org/10.1515/hsz-2019-0368.
Ramezanian, M.S., Padmaja, S., Koppenol, W.H., 1996. Nitration and hydroxylation of phenolic compounds by peroxynitrite. Chem. Res. Toxicol. 9, 232–240. https://doi.org/10.1021/tx950135w.
Sedlacek, C.J.; Giguere, A.T.; Dobie, M.D.; Mellbye, B.L.; Ferrell, R.V.; Woebken, D.; Sayavedra-Soto, L.A.; Bottomley, P.J.; Daims, H.; Wagner, M.; Pjevac, P. Transcriptomic response of Nitrosomonas europaea transitioned from ammonia- to oxygen-limited steady-state growth. mSystems, 5 (2020), pp., https://doi.org/10.1128/mSystems.00562-19https://doi.org/.
Shi, J., Fujisawa, S., Nakai, S., Hosomi, M., 2004. Biodegradation of natural and synthetic estrogens by nitrifying activated sludge and ammonia-oxidizing bacterium *Nitrosomonas europaea*. Water Res. 38, 2322–2329. https://doi.org/10.1016/j.watres.2004.02.022.
Shraddha, Shekher, R., Sehgal, S., Kamthania, M., Kumar, A., 2011. Laccase: microbial sources, production, purification, and potential biotechnological applications. Enzyme Res. 1–11. https://doi.org/10.4061/2011/217861.
Skotnicka-Pitak, J., Khunjar, W.O., Love, N.G., Aga, D.S., 2009. Characterization of metabolites formed during the biotransformation of 17α-ethinylestradiol by *Nitrosomonas europaea* in batch and continuous flow bioreactors. Environ. Sci. Technol. 43, 3549–3555. https://doi.org/10.1021/es8026659.
Soliman, M., Eldyasti, A., 2018. Ammonia-oxidizing bacteria (AOB): opportunities and applications—a review. Rev. Environ. Sci. Biotechnol. 17, 285–321. https://doi.org/10.1007/s11157-018-9463-4.
Starkenburg, S.R., Arp, D.J., Bottomley, P.J., 2008. Expression of a putative nitrite reductase and the reversible inhibition of nitrite-dependent respiration by nitric oxide in *Nitrobacter winogradskyi* Nb-255. Environ. Microbiol. 10, 3036–3042. https://doi.org/10.1111/j.1462-2920.2008.01763.x.
Sun, Y., Chen, Z., Wu, G., Wu, Q., Zhang, F., Niu, Z., Hu, H.-Y., 2016. Characteristics of water quality of municipal wastewater treatment plants in China: implications for resources utilization and management. J. Clean. Prod. 131, 1–9. https://doi.org/10.1016/j.jclepro.2016.05.068.
Tetreault, G.R., Bennett, C.J., Shires, K., Knight, B., Servos, M.R., McMaster, M.E., 2011. Intersex and reproductive impairment of wild fish exposed to multiple municipal wastewater discharges. Aquat. Toxicol. 104, 278–290. https://doi.org/10.1016/j.aquatox.2011.05.008.
Vader, J.S., van Ginkel, C.G., Sperling, F.M.G.M., de Jong, J., de Boer, W., de Graaf, J.S., van der Most, M., Stokman, P.G.W., 2000. Degradation of ethinyl estradiol by nitrifying activated sludge. Chemosphere 41, 1239–1243. https://doi.org/10.1016/S0045-6535(99)00556-1.
Wang, B., Ni, B.J., Yuan, Z., Guo, J., 2019a. Cometabolic biodegradation of cephalexin by enriched nitrifying sludge: Process characteristics, gene expression and product biotoxicity. Sci. Total Environ. 672, 275–282. https://doi.org/10.1016/j.scitotenv.2019.03.473.
Wang, B., Ni, B.J., Yuan, Z., Guo, J., 2019b. Insight into the nitrification kinetics and microbial response of an enriched nitrifying sludge in the biodegradation of sulfadiazine. Environ. Pollut. 255, 113160 https://doi.org/10.1016/j.envpol.2019.113160.
Wijma, H.J., Canters, G.W., de Vries, S., Verbeet, M.P., 2004. Bidirectional catalysis by copper-containing nitrite reductase. Biochemistry 43, 10467–10474. https://doi.org/10.1021/bi0496687.
Yi, T., Harper Jr., W.F., 2007. The link between nitrification and biotransformation of 17alpha-ethinylestradiol. Environ. Sci. Technol. 41, 4311–4316. https://doi.org/10.1021/es070102q.
Yu, R., Chandran, K., 2010. Strategies of *Nitrosomonas europaea* 19718 to counter low dissolved oxygen and high nitrite concentrations. BMC Microbiol. 10, 70. https://doi.org/10.1186/1471-2180-10-70.
Yu, Y., Han, P., Zhou, L.J., Li, Z., Wagner, M., Men, Y., 2018. Ammonia monooxygenase-mediated cometabolic biotransformation and hydroxylamine-mediated abiotic transformation of micropollutants in an AOB/NOB coculture. Environ. Sci. Technol. 52, 9196–9205. https://doi.org/10.1021/acs.est.8b02801.
Zhang, Q.H., Yang, W.N., Ngo, H.H., Guo, W.S., Jin, P.K., Dzakpasu, M., Yang, S.J., Wang, Q., Wang, X.C., Ao, D., 2016. Current status of urban wastewater treatment plants in China. Environ. Int. 92–93, 11–22. https://doi.org/10.1016/j.envint.2016.03.024.